bioRxiv preprint first posted online Jul. 26, 2016; doi: http://dx.doi.org/10.1101/066043. The copyright holder for this preprint (which was not peer-reviewed) is the author/funder. All rights reserved. No reuse allowed without permission.

Title: False Negatives Are a Significant Feature of Next Generation Sequencing Callsets

Authors: Dean Bobo[1], Mikhail Lipatov[1], Juan L. Rodriguez-Flores[2], Adam Auton[3] and Brenna M. Henn[1,4§]

[1] Department of Ecology and Evolution, Stony Brook University, Stony Brook, NY, 11794, USA.
[2] Department of Genetic Medicine, Weill Cornell Medical College. New York, NY, 10021, USA.
[3] Department of Genetics, Albert Einstein College of Medicine, Bronx, NY, 10461, USA.
[4] Graduate Program in Genetics, Stony Brook University, Stony Brook, NY, 11794, USA.

[§] Correspondence should be addressed to: Brenna Henn, Dept. of Ecology and Evolution, Life Sciences Bldg., Room 640, Stony Brook NY 11794. Phone: 631-632-1412.
E-mail: brenna.henn@stonybrook.edu

Key Words: sequencing error, mutation rate, de novo mutations, next-generation sequencing

Data deposition: Data and software are freely available on the Henn Lab website: https://ecoevo.stonybrook.edu/hennlab/data-software/

Software: GITHUB via https://ecoevo.stonybrook.edu/hennlab/data-software/

bioRxiv preprint first posted online Jul. 26, 2016; doi: http://dx.doi.org/10.1101/066043. The copyright holder for this preprint (which was not peer-reviewed) is the author/funder. All rights reserved. No reuse allowed without permission.

Abstract:

Short-read, next-generation sequencing (NGS) is now broadly used to identify rare or *de novo* mutations in population samples and disease cohorts. However, NGS data is known to be error-prone and post-processing pipelines have primarily focused on the removal of spurious mutations or "false positives" in downstream genome datasets. Less attention has been paid to characterizing the fraction of missing mutations or "false negatives" (FN). We design a phylogeny-aware tool to determine false negatives [PhyloFaN] and describe how read coverage and reference bias affect the FN rate. Using thousand-fold coverage NGS data from both Illumina HiSeq and Complete Genomics platforms derived from the 1000 Genomes Project, we first characterize the false negative rate in human mtDNA genomes. The false negative rate for the publically available callsets is 17-20%, even for extremely high coverage haploid data. We demonstrate that high FN rates are not limited to mtDNA by comparing autosomal data from 28 publically available full genomes to intergenic Sanger sequenced regions for each individual. We examine both low-coverage Illumina and high-coverage Complete Genomics genomes. We show that the FN rate varies between ~6%-18% and that false-positive rates are considerably lower (<3%). The FN rate is strongly dependent on calling pipeline parameters, as well as read coverage. Our results demonstrate that missing mutations are a significant feature of genomic datasets and imply additional fine-tuning of bioinformatics pipelines is needed. We provide a tool which can be used to quantify the FN rate for haploid genomic experiments, without additional generation of validation data.

bioRxiv preprint first posted online Jul. 26, 2016; doi: http://dx.doi.org/10.1101/066043. The copyright holder for this preprint (which was not peer-reviewed) is the author/funder. All rights reserved. No reuse allowed without permission.

Report

Mutation is the process by which novel genetic variation is generated; thus, the accurate identification of mutations in genomic data is of the utmost importance for mapping Mendelian disease, population genetic analysis, tumor sequencing, and rare variant phenotype/genotype associations[1]. Multiple bioinformatic algorithms have been developed to call mutations from short read, next-generation sequencing (NGS) data[2,3]. However, there is a growing consensus that both short- and long-read NGS associated calling methods generate datasets with appreciably high error rates, particularly for rare or *de novo* mutations[4-6]. These technical error profiles affect many forms of human genomic data, and are particularly crucial for the identification of *de novo* mutations in disease phenotypes[7-9] and somatic tissue[10,11]. Raw 2nd generation sequencing read data contains a great number of false positive variants (i.e. referred to as "sequencing error"[12]). Accordingly, pre- and post-processing pipelines filter the raw data in order to discard false positive variants. However, such pipelines may also miss true variants, which will then result in a relatively high false negative rate in the variant callset.

Recent efforts to quantify NGS error rates have primarily been focused on the identification of false positive errors in human NGS data[13,14]. However, the need for the quantification of false negatives in such data has received far less attention[15,16]. High error rates complicate disease studies which search for *de novo* disease mutations between parents and probands with exome or genome sequencing. There is often a high number of candidate *de novo* mutations identified in trio/duo, but most candidates are a result of either a false positive in the offspring or a false negative in a parent [17-19]. For example, Vissers *et al.* [19] identify 51 candidate *de novo* mutations in ten probands with mental retardation, but were only able to validate 13 with Sanger sequencing. Sanger validation of the parents revealed that only 9 of these were truly *de novo*, the remaining 4 were likely false negatives in the parents (i.e. 30% false negative rate). Other studies identify similarly high false negative rates[20], but the precise ratio will depend on many factors. For example, in the context of trio-calling, filtering for mutations which are already present in a large SNP repository, such as dbSNP, will mean that recurrent *de novo* mutations are eliminated from the final callset; recent work with the EXaC database specifically highlights this problem[21]. Recently, Chen *et al.*[22] report that damage introduced in-vitro during NGS library preparation results in a high number of spurious variants, and estimate that this damage causes the majority of G to T transversions in 73% of large, publically available datasets (i.e. 1000G and the Cancer Genome Atlas [TCGA]). A balanced assessment of both false positive and false negative error rates is necessary for Mendelian and complex disease identification approaches, but also crucial for evolutionary studies of mutation rates[5].

We present a new phylogeny-based method to identify false negative errors in mtDNA callsets *without* generating additional validation data. The sequences used by our method must be both homologous and non-recombining so that a single, non-ambiguous phylogeny can be constructed. This approach can be broadly used to optimize the FN rate in human next-generation sequencing experiments as set by the user. We apply our method to single nucleotide variants (SNVs) in human mitochondrial NGS data for more than 2,500 individuals. We reconsider germline mutation rate estimation in the context of false negatives by identifying *de novo* mutations from 131 mother/child duos from 1000

bioRxiv preprint first posted online Jul. 26, 2016; doi: http://dx.doi.org/10.1101/066043. The copyright holder for this preprint (which was not peer-reviewed) is the author/funder. All rights reserved. No reuse allowed without permission.

Genomes Phase 3 Complete Genomics data. We find that many candidate *de novo* mutations are spurious due to a combination of false positive variants identified in the child and/or missed variants (false negatives) in the mother. Our results are in general agreement with the rates that have been calculated in previous Sanger sequencing studies[23] if we aggressively filter the dataset.

In addition to calculating the false negative rate by leveraging phylogenies, we also empirically measured the false negative and false positive rates from published autosomal NGS data (from the 1000 Genomes Project [1000G] and Human Genome Diversity Panel [HGDP]) via Sanger-based sequencing validation[24]. In total, we compare NGS data for 6 Mbuti (MBI) samples from HGDP, 16 Luhya (LWK) from 1000 Genomes Project and 6 Yoruba (YRI) from Complete Genomics samples for which intergenic Sanger sequencing was also available.

mtDNA FN identification

To identify false negative variants without generating additional experimental data, we leverage the phylogenetic nature of genetic sequences. In the absence of recombination, any given contiguous sequence of nucleotides can be modeled as being inherited identically by descent (IBD) by creating a phylogenetic tree of shared and derived mutations. In the absence of repeat mutation, any two DNA sequences with a recent common ancestor will share a set of mutations IBD, as well as carry their own unique and derived mutations. Using a detailed public mtDNA phylogeny (phylotree.org), we identified all variants shared by multiple mtDNA genomes such that they form the internal branches of the phylogeny. These mtDNA variants have been identified via Sanger sequencing; over the past 15 years, over 20,000 mtDNA genomes have deposited in NCBI and carefully curated by a variety of consortiums (phylotree.org, mitomap.org). We estimate the false negative rate for each sample by assigning a next-generation sequenced individual to a haplogroup in the phylogeny, and count the number of missed variants using the known set of mutations for the assigned haplogroup (see **Figure 1**). It is important to note that mutations on terminal branches are excluded, as we do not know whether these maybe private to the given sample used to build the tree. In addition, the rate of back mutation is assumed to be negligible but could be implemented in this model. HaploGrep was designed to be robust haplogroup assignment tool, considering the entire mitochondrial genome or any subset of it[25]. As such, even if a variant that defines a large clade on the phylogenetic tree is removed, HaploGrep is still able to accurately place the genome in the proper haplogroup, albeit with a lower confidence score. Therefore, we can still use the phylogenetic nature of the mitochondrial genome to identify missing variants.

False negative estimates were calculated for two different sequencing platforms: 393 individuals in pedigree trios were sequenced by Complete Genomics[26] and 2,535 individuals from the 1000 Genomes Phase 3 dataset[27] sequenced via Illumina HiSeq platforms. Many individuals that were sequenced with Complete Genomics were also sequenced in the 1000 Genomes dataset allowing us to directly compare the false negative rate between the two platforms. The Complete Genomics data contained variants (up to about 50 base pairs in length) called via the company's assembly pipeline with respect to the revised Cambridge Reference Sequence (rCRS) of the human mitochondrial genome[28,29]. The Illumina dataset consisted of mitochondrial genomes

bioRxiv preprint first posted online Jul. 26, 2016; doi: http://dx.doi.org/10.1101/066043. The copyright holder for this preprint (which was not peer-reviewed) is the author/funder. All rights reserved. No reuse allowed without permission.

sequenced using 75 - 100 bp paired-end reads that were mapped using the Burrows-Wheeler Aligner (BWA) software[30]. Variant calling by the 1000 Genomes Consortium was performed with the Genome Analysis Toolkit (GATK) software[2,31]. During preparation of the callset, it was assumed that for any given locus the mtDNA has only one allele in a particular individual and heterozygous sites were removed.

We developed a software tool, PhyloFaN, that accepts VCF or VAR files as input data and is capable of lifting over variants detected using hg19 reference genome to the rCRS mitochondrial reference genome; variants detected with GRCh37 (NC_012920) do not require liftover to rCRS as the mitochondrial sequences are identical. Once input variants are aligned to match the rCRS numbering convention, both insertions and deletions are removed from the sample callset and complex multi-nucleotide polymorphisms and multi-allelic sites are split into individual records. Mitochondrial haplogroups are then assigned to each sample using the HaploGrep algorithm[25] according to the mtDNA phylogenetic tree[32].

We isolate the expected internal variants for each sample based on its assigned haplogroup, and computed the rate in which haplogroup-defining variants were not observed. This rate is computed with a Bayesian inference routine, the Bernoilli *p* is used with a Jeffreys prior. The number of Bernoulli experiments, *n*, is represented as the number expected variants, given its haplogroup assignment, and the number of successes, *k*, is represented by the number of variants out of the expected that were found.

In the Complete Genomics dataset, our algorithm estimates that 2,313 out of 11,429 predicted variants were missing from the NGS variant callset. This corresponds to a false negative rate of 20.2% (credible interval, CI: 19.5%-21.0%). We repeated the procedure for the Illumina mtDNA and obtained a false negative rate of 21.3% (95% C.I. between 21.1% and 21.5%). The ~2,300 variants identified as missing in the Complete Genomics data and the ~18,100 variants identified as missing in the Illumina data are plotted according to their mitochondrial base pair location (**Figure 2**). False negatives are particularly enriched in the hypervariable regions, despite excluding indels from the FN calculation. The tandem repeats in the hypervariable region could cause an increase in *de novo* mutations due to replication slippage, which is common in an origin of replication with a repetitive nature. However, false negatives were not enriched in regions of repetitive sequence as identified with RepeatMasker (regions shown in **Figure 2**). Higher mutation rate in this region could be responsible for a fraction of the apparent ‘false negatives’ observed using this model (but see below).

We investigated whether the loss of these putative true variants from the callset was due to the strictness of filters applied by the post-processing pipelines. Such pipelines tend to optimize filtering out false positive variants, which are highly prevalent in raw 2nd generation sequencing data[2,33]. We hypothesized that these pipelines would often miss large numbers of variants that are, in truth, present within the raw sequence data. We confirmed that the missing variants were indeed present in the pre-pipeline BAM files. For example, the HaploGrep algorithm assigns individual HG00097 to haplogroup T2f1a1. The mitochondrial phylogeny has a substitution from G to A at position 8860 (rs2001031) derived in the reference sequence haplogroup, H2a2. Thus, the phylogeny predicts that the mitochondrial sequence of HG00097 would to have a G at this locus, whereas the reference sequence has an A. This G variant was not present in the

bioRxiv preprint first posted online Jul. 26, 2016; doi: http://dx.doi.org/10.1101/066043. The copyright holder for this preprint (which was not peer-reviewed) is the author/funder. All rights reserved. No reuse allowed without permission.

sample VCF file but was indeed present in the original BAM file for this sample (**Figure S1**).

The variant at location 8860 contributes to the false negative rate in our case study to a great extent due to the fact that it defines the H2a2 haplogroup of the Cambridge Reference Sequence. It is predicted but missing in 2,533 of the 2,535 Illumina VCF files. As a result, the corresponding 2,533 false negative calls comprise 17% of the false negatives we detect in the Illumina callset. This variant represents the central peak in **Figure 2**. We also checked whether the exclusion of multi-allelic variants in the public 1000G Illumina mtDNA files significantly affects the FN rate. Here, "multi-allelic" is defined as a locus that has more than two alleles present among the sampled individuals. As per our expectation, allowing for multi-allelic variants in the VCF improved the false negative rate, decreasing from 21.3% to 17.1% (C.I.: 16.8%-17.3%). Multi-allelic variants may be more common in mtDNA datasets than autosomal due to high relative mutation rate of mtDNA.

We further investigated the effect of decreasing the number of stringency filters in the GATK pipeline on the false negative rate. Specifically, we recalled variants using the original BAM files using GATK's UnifiedGenotyper[31] with respect to the GRCh37 reference sequence. The choice of reference genome is significant because most variant calling pipelines align to a reference genome from which non-reference variants are identified; FN's are, by default, assumed to carry the reference allele[15,34]. We ran GATK default emit-all parameters (i.e. permissive genotype calling) on each individual sample separately (referred to as "single-sample calling"). This pipeline dramatically reduced the false negative rate in Illumina data, from 17.1% down to 2.28%. We note that is approach is likely associated with a great number of false positive variant calls because these filters are built to minimize sequencing error in autosomal sequences – but the experiment demonstrates how the majority of the false negatives are present in the short read data and erroneously excluded in subsequent filtering processes. In summary, we find that most FN variants are missing due to filtering within the post-processing pipeline.

We then tested whether false negative status of a variant correlates with short read coverage. To compute the depth of coverage for each base pair location in each sample in our Illumina data, we used GATK's DepthOfCoverage[31]. Average coverage for the variants identified as false negatives was found to be 2,022x, while that for the variants expected from the phylogeny and contained in the VCF files was 2,244x. The difference between coverage values of the former group and those of the latter group was shown to be significant by a t-test ($p < 2.2\times10^{-16}$, 95% C.I. for the difference in coverage between 197x and 248x). A best-fit logit linear regression model of the dependence of false negative status on coverage based on the same data had an intercept equal to -1.36 and a coefficient of the explanatory variable equal to -0.000105. A logit model with these parameters predicts that an increase in coverage from 2,000 to 3,000 reads leads to a decrease in the probability of false negative status from 17.3% to 15.8%. In other words, for our extremely high-coverage data, the effect of coverage on the false negative error status via the pipeline filters is significant but not very large.

Estimating error rates using Sanger sequencing data

Our phylogenetic approach is currently confined to non-recombining homologous loci, such as mtDNA and the Y chromosome. While PhyloFaN can be used to

bioRxiv preprint first posted online Jul. 26, 2016; doi: http://dx.doi.org/10.1101/066043. The copyright holder for this preprint (which was not peer-reviewed) is the author/funder. All rights reserved. No reuse allowed without permission.

systematically explore the effect of pipeline parameters on the false negative using haploid systems, it is an imperfect proxy for assaying autosomal data. Future extensions using ancestral recombination graphs[35], however, hold great potential. We nonetheless verified the ubiquity of false negatives in autosomal next-generation sequence data by a more conventional approach, comparing NGS variant calls to Sanger-based sequencing. We compare public variant call datasets from Illumina and Complete Genomics genomes to an independently published Sanger-sequencing experiment[36], performed on the same individuals (*see below*, all samples are cell-line derived). This Sanger data consists of short 2 kilobase intervals distributed at 40 loci throughout the autosomes. These loci were previously chosen to estimate neutral genetic diversity in human populations and hence are located at some distance from genes[36]. These Sanger data differ from prior experiments because they were not chosen merely to validate specific NGS variants, as typically occurs for most NGS validation experiments. Hence, they represent an unbiased estimate of the false negative and false positive rates. Comparable NGS and Sanger sequence data were available for 6 Mbuti (MBI), 6 Yoruba (YRI) and 16 Luhya (LWK) [36].

We obtained comparable next-generation sequencing data from 28 human genomes sequenced as part of the Human Genome Diversity Project[37], Complete Genomics public dataset and the 1000 Genomes Project[38]. The forty 2 kilobase intergenic Sanger sequences for 28 individuals were independently aligned to the reference genome (GRCh37) using BLAST. We designed a Perl script that used the BLAST trace-back operation (BTOP) string to generate a VCF file. For consistency, we excluded indels from this analysis so the autosomal and mitochondrial false negative rates could be compared. We ensured that both Sanger sequences (one per chromosome) had the same start and stop position and manually trimmed problem alignments if necessary (**Figure 1B**). We compared the Sanger sequences to single-sample called and multi-sampled called variants, as well as imputed and unimputed versions of these callsets (**Table 1**). In order to generate single-sample callsets for the 1000 Genomes and HGDP data, we used accessed available BAM files and generated VCFs using GATK's Genotyper (-stand_emit_conf 30; -stand_call_conf 30). Emit-all files were generated so depth information would be available at all sites. Sites that fall below the stand_emit_conf or stand_call_conf are still emitted but with a LowQual flag. Complete Genomics variant data were only publically available from their proprietary single-sample calling pipeline.

We count false negatives by comparing variants identified by Sanger sequencing to NGS. Each site receives a score of 0, 1, or 2: 0 indicates concordance between the Sanger and NGS genotype call, a score of 1 indicates that one alternate allele was not identified by NGS, and a score of 2 indicates that both alternate alleles were missed by NGS. To calculate the false negative rate for a sample, the scores for each site are totaled and divided by the number of expected calls, that is, the number of alternate alleles from the Sanger sequencing and multiplied by 100. Imputation is expected to identify highly probable genotypes that were absent in an initial dataset; imputation is a standard "refinement" feature of large genome datasets – including publically available 1000G and HGDP. We therefore score imputed and unimputed datasets differently, penalizing missing variants in an imputed dataset even if there is no coverage at the locus (see **Table S1**). In addition, we penalize sites in our single-sample emit-all VCFs that were called variants but marked with LowQual, as these variants would not be included in a typical

bioRxiv preprint first posted online Jul. 26, 2016; doi: http://dx.doi.org/10.1101/066043. The copyright holder for this preprint (which was not peer-reviewed) is the author/funder. All rights reserved. No reuse allowed without permission.

variant-only file. We count false positives and the false positive rate using a similar scoring system. A score of 0 at a given site indicates concordance between the NGS and Sanger variants, a score of 1 indicates that one alternate allele was identified by NGS as variant but was reference in the Sanger data, and a score of 2 indicates that a site was called homozygous alternative by NGS and homozygous reference by Sanger.

False Negative and False Positive Autosomal Rates for Public NGS Callsets

We first examine the single sample called variants for all three datasets. The 1000 Genomes and HGDP data represent low coverage autosomal datasets (~7x) (*Supplementary Information, Table S1*), while Complete Genomics represents a high coverage dataset (~54x). We expect the high coverage data to have significantly lower FN rates due to enhanced read coverage. In the 1000G LWK samples, we observe an average false negative rate of 18.3% in the unimputed single-sample callset (**Table 1**). In the HGDP Mbuti samples, the observed mean false negative rate was 7.6% in the single-sample callset. The observed Complete Genomics YRI genomes single-sample FN rate was 5.7% (**Table 1**). Our results indicate a significant difference between the single-sample calling of the 1000G false negative rate (18.3%) and the HGDP false negative rate (7.6%) which may be due to factors including library preparation, read length, sequencing instrument sensitivity, and base or variant recalibration. Both callsets were generated using parameters as specified in GATK's best practices documentation. The coverage was marginally higher on average in the 1000G dataset (7.43x) than HGDP (6.71x). Surprisingly, the high coverage CG data had a FN rate nearly identical to the low coverage HGDP genomes. This demonstrates that *coverage alone* is not the primary determinant of FNs in a dataset; other factors, likely variant filters and sequencing technology[12] are important determinants.

False negatives are common at low coverage sites but are also observed at higher coverage sites in our dataset, e.g. 17x in a LWK individual (NA19307, chr4, position 27450119) (**Figure S2**). With biallelic sampling, the probability of sequencing only one gamete 17 times is very low (p=7.6*10^{-6}); however, given the large number of sites obtained from whole genome sequencing the expected number of sites obtained from only a single gamete is still very large (e.g. ~19,000 assuming even 17x coverage of 2.5Gb). Not all of these sites, however, will contain a non-reference variant. We systematically investigated the range of coverage for false negative variants identified from the single-sample called datasets (**Figure 3**). It is important to note that we do not call a site FN in the single-sample callset if there is 0x coverage; however, if there were sufficient reads present for the emit-all determination of a reference allele, then we do consider the site in our FN rate. We observe FNs at a range of coverages, most of the Illumina FNs were covered by 4x or more reads (**Figure 3, S2**). Coverage is far less variable in the smaller Complete Genomics dataset, but we still observe false negatives at ~40x to almost 90x coverage. Contrary to our expectation, we find that the allele frequency for a variant is not a good proxy for estimating the probability of a false negative given there is almost an even distribution of false negatives across all allele frequencies in our sample population (**Figure S3**).

Imputation is often used to 'fill-in' missing variants that may be present at appreciable frequency in a genomic dataset but are missing in a given individual due to variation in coverage or stochastic sampling. We considered the FN rates in multi-sample

bioRxiv preprint first posted online Jul. 26, 2016; doi: http://dx.doi.org/10.1101/066043. The copyright holder for this preprint (which was not peer-reviewed) is the author/funder. All rights reserved. No reuse allowed without permission.

called and imputed datasets. In the 1000 Genomes LWK samples, we observe an average FN rate of 5.9% in the imputed multi-sample callset (**Table 1**). We were unable to calculate the FN in a multi-sample unimputed dataset for these LWK samples as 1000 Genomes does not make this variant dataset publically available. In the HGDP Mbuti samples that were imputed and multi-sample called, we observe an 8.8% FN rate but a 3.3% FN rate in multi-sample unimputed calls (see **Table 1**).

Finally, we also calculated the false positive rates for these samples using the same Sanger dataset in order to assess potential trade-offs in sensitivity versus specificity (**Table 1**, **Figure S4**). False positive rates were indeed much lower than FN rates, indicating that calling pipelines implemented for these public datasets were optimized for reducing false positives. The 1000G single-sample dataset has a false positive rate of 2.2% and is further reduced in the imputed multi-sample calls to 0.6%. The HGDP callsets have false positive rates of 2.9% in the single-sample callset, 1.2% in the multi-sample unimputed callset, and 1.1% in the multi-sample imputed dataset. We did not observe a single FP in the Complete Genomics dataset, suggesting that the CG variant calling pipeline strongly optimizes for accurate specificity of FPs.

mtDNA de novo mutation rate

Our results indicate that the false negative rate is sensitive to variant filtering and coverage, leading to false negative rates of 6-20% for publically available datasets. We illustrate the effect of the FN rate by considering its impact on estimates of the human mtDNA germline mutation rate. We estimate the germline mtDNA mutation rate by comparing mitochondrial genomes of mothers with those of their children to identify *de novo* mutations. We utilize 131 mother-child pairs from the 1000 Genomes Phase 3 Complete Genomics samples[27] for which genotype calls were provided by proprietary CG processing pipelines. We identified 36 mitochondrial SNVs that were present in the child but not in the mother (**Table 2**). For each mother-child pair that had a putative *de novo* mutation, we used HaploGrep to assign haplogroups on the basis of the known mitochondrial phylogenetic tree[25,32], separately for both the mother and the child.

Next, to confirm maternal assignment for each duo, we compared the haplogroups that HaploGrep assigned to the mother and the child for each of the pairs. We retain pairs for which either (a) the mother's haplogroup was the same as the child's, (b) the child's haplogroup was contained within the mother's or (c) the mother's haplogroup was contained within the child's. Two of the 34 candidate *de novo* mutations came from mother-child pairs whose haplogroup pairs did not fall in either of the above-mentioned categories indicating sample swaps or non-maternity. For each of the remaining candidate mutations, we then checked the variant call in the mother's data. We excluded 15 candidate *de novo* mutations that had been identified within segments that had a 'no-call' status in the mother (**Table 2**). We then applied our phylogenetic method of identifying false negatives to each of the remaining 19 candidate *de novo* mutations to test whether the absence of each of these variants in the mother's sequence was due to a false negative call at the locus in question. For 9 of the remaining candidate mutations, the variants in the mother's sequence were predicted to be present based on the mother's phylogenetic lineage, so the corresponding candidate mutations were excluded. This left us with 10 candidate *de novo* mutations: 8 in the coding region and 2 in the control region.

bioRxiv preprint first posted online Jul. 26, 2016; doi: http://dx.doi.org/10.1101/066043. The copyright holder for this preprint (which was not peer-reviewed) is the author/funder. All rights reserved. No reuse allowed without permission.

In order to assess whether our final *de novo* mutation candidates could still be false positives, we compared their variant quality scores (varScoreVAF column in the Complete Genomics VAR files for children that had the corresponding SNVs) with those of all SNVs identified in our Complete Genomics data (**Figure S5**). The ten *de novo* mutation candidates have significantly lower variant quality scores than the rest of the SNVs in the dataset (Mann-Whitney test, $p = 0.02$) indicating that many of them are likely spurious variants. Only 4 variants had a varScoreVAF (derived from maximum likelihood model) greater than 5000.

Using the 131 duo dataset, we could then compare the NGS mtDNA coding region mutation rate with earlier Sanger sequencing estimates. By dividing the number of putative *de novo* mutations by the total called sequence length (see *Supplemental Methods*), we obtain an estimate of $8 / 1{,}981{,}090 = 4.04\times10^{-6}$ mutations per base pair per generation (95% CI: 1.74×10^{-6} - 7.96×10^{-6}) in the human mitochondrial coding region and $2 / 146{,}610 = 1.36\times10^{-5}$ mutations per base pair per generation in the control region (95% CI: 1.65×10^{-6} and 4.93×10^{-5}). However, if we consider only the two coding region mutations which have a quality score greater than 5000, then we obtain an estimate of $\mu = 1.01\times10^{-6}$/bp/g. Howell and colleagues[23] produce a Sanger pedigree-based estimate of the coding region mutation rate of 6.0×10^{-7} bp/g (99.5% CI: 8.0×10^{-8} - 2.0×10^{-6} bp/g), after conversion from the divergence rate to the mutation rate and assuming 20 years per generation; inclusion of all 8 mutations in Table 1 results in a mutation rate outside of the earlier confidence interval, while our more conservative 1.01×10^{-6}/bp/g is consistent with Howell et al.'s meta-analysis. A recent mtDNA genome μ estimate of 2.7×10^{-7}/bp/g from extremely high coverage NGS sequencing of 39 mother-child duos is significantly lower than the pedigree estimate here; however Rebolledo-Jaramillo et al.[39] note that they heavily filtered variant calls in order to confidently discern heteroplasmies from sequencing artifacts, and therefore their estimate should be seen as a lower bound. We note that multi-generational pedigrees are needed to discriminate *de novo* germline mutations from somatic mutations. Assuming that the true FN detection rate in the CG dataset is ~20%, one could also argue that our μ should be corrected by 20% to account for missing *de novo* variant calls in the child (**Table S2**).

Conclusions:

We demonstrate that false negative mutations are significant feature of short-read, next-generation sequencing data sets. Gross characterization of the expected false negative rate is difficult because the FN rate is primarily sensitive to post-processing variant calling pipeline parameters. Previously, these pipeline parameters have been optimized for false positive removal (**Table 1**). We provide a computational tool [PhyloFaN] for rapid estimation of the FN rate in new genomic datasets, which will allow optimization of the FN rate without relying on new Sanger sequencing data. Autosomal FN results presented here range between 6%-18% for large publically available genome datasets. While 80 total kilobases per individual contains relatively few SNPs, our approach is unique for using an unbiased dataset that was not chosen to specifically validate *de novos*. Finally, we explore implications of FNs and FPs in 131 high-coverage mtDNA duos from 1000 Genomes. We find that the majority (89%) of putative *de novos* identified in the child are due to either variant quality issues or false negatives in the mother (resulting in a 'false positive' *de novo* for the child). Accurate identification of *de*

bioRxiv preprint first posted online Jul. 26, 2016; doi: http://dx.doi.org/10.1101/066043. The copyright holder for this preprint (which was not peer-reviewed) is the author/funder. All rights reserved. No reuse allowed without permission.

novo mutations remains a critical challenge for Mendelian disease, cancer genomics and mutation rate estimation.

Acknowledgements: We thank Krishna Veeramah for providing the Sanger sequencing dataset. We thank Adam Siepel and Vagheesh Narasimhan for valuable discussion. Finally, we are grateful to Jason O'Rawe for coding the mtDNA false negative pipeline. D.B. was supported by The Research Foundation at SUNY Stony Brook.

bioRxiv preprint first posted online Jul. 26, 2016; doi: http://dx.doi.org/10.1101/066043. The copyright holder for this preprint (which was not peer-reviewed) is the author/funder. All rights reserved. No reuse allowed without permission.

References:

1. Shendure, J., and Akey, J.M. (2015). The origins, determinants, and consequences of human mutations. Science *349*, 1478–1483.

2. DePristo, M.A., Banks, E., Poplin, R., Garimella, K.V., Maguire, J.R., Hartl, C., Philippakis, A.A., del Angel, G., Rivas, M.A., Hanna, M., et al. (2011). A framework for variation discovery and genotyping using next-generation DNA sequencing data. Nature Genetics *43*, 491–498.

3. Ramu, A., Noordam, M.J., Schwartz, R.S., Wuster, A., Hurles, M.E., Cartwright, R.A., and Conrad, D.F. (2013). DeNovoGear: de novo indel and point mutation discovery and phasing. Nat Meth *10*, 985–987.

4. Wall, J.D., Tang, L.F., Zerbe, B., Kvale, M.N., Kwok, P.-Y., Schaefer, C., and Risch, N. (2014). Estimating genotype error rates from high-coverage next-generation sequence data. Genome Research *24*, 1734–1739.

5. Ségurel, L., Wyman, M.J., and Przeworski, M. (2014). Determinants of Mutation Rate Variation in the Human Germline. Annu. Rev. Genom. Human Genet. *15*, 140626174348008.

6. O'Rawe, J.A., Ferson, S., and Lyon, G.J. (2015). Accounting for uncertainty in DNA sequencing data. Trends in Genetics *31*, 61–66.

7. Kong, A., Frigge, M.L., Masson, G., Besenbacher, S., Sulem, P., Magnusson, G., Gudjonsson, S.A., Sigurdsson, A., Jonasdottir, A., Jonasdottir, A., et al. (2012). Rate of de novo mutations and the importance of father's age to disease risk. Nature *488*, 471–475.

8. Ng, S.B., Bigham, A.W., Buckingham, K.J., Hannibal, M.C., McMillin, M.J., Gildersleeve, H.I., Beck, A.E., Tabor, H.K., Cooper, G.M., Mefford, H.C., et al. (2010). Exome sequencing identifies MLL2 mutations as a cause of Kabuki syndrome. Nature Publishing Group *42*, 790–793.

9. Bamshad, M.J., Ng, S.B., Bigham, A.W., Tabor, H.K., Emond, M.J., Nickerson, D.A., and Shendure, J. (2011). Exome sequencing as a tool for Mendelian disease gene discovery. Nature Reviews Genetics *12*, 745–755.

10. Tomasetti, C., Vogelstein, B., and Parmigiani, G. (2013). Half or more of the somatic mutations in cancers of self-renewing tissues originate prior to tumor initiation. Proceedings of the National Academy of Sciences *110*, 1999–2004.

11. Costa, H.A., Leitner, M.G., Sos, M.L., Mavrantoni, A., Rychkova, A., Johnson, J.R., Newton, B.W., Yee, M.-C., La Vega, De, F.M., Ford, J.M., et al. (2015). Discovery and

bioRxiv preprint first posted online Jul. 26, 2016; doi: http://dx.doi.org/10.1101/066043. The copyright holder for this preprint (which was not peer-reviewed) is the author/funder. All rights reserved. No reuse allowed without permission.

functional characterization of a neomorphic PTEN mutation. Proceedings of the National Academy of Sciences *112*, 13976–13981.

12. Robasky, K., Lewis, N.E., and Church, G.M. (2013). The role of replicates for error mitigation in next-generation sequencing. Nature Reviews Genetics *15*, 56–62.

13. Zook, J.M., Chapman, B., Wang, J., Mittelman, D., Hofmann, O., Hide, W., and Salit, M. (2014). Integrating human sequence data sets provides a resource of benchmark SNP and indel genotype calls. Nature Biotechnology *32*, 246–251.

14. Kennedy, B., Kronenberg, Z., Hu, H., Moore, B., Flygare, S., Reese, M.G., Jorde, L.B., Yandell, M., and Huff, C. (2014). Using VAAST to Identify Disease-Associated Variants in Next-Generation Sequencing Data. Curr Protoc Hum Genet *81*, 6.14.1–.14.25.

15. Brandt, D.Y.C., Aguiar, V.R.C., Bitarello, B.D., Nunes, K., Goudet, J., and Meyer, D. (2015). Mapping Bias Overestimates Reference Allele Frequencies at the HLA Genes in the 1000 Genomes Project Phase I Data. G3 (Bethesda) *5*, 931–941.

16. Pabinger, S., Dander, A., Fischer, M., Snajder, R., Sperk, M., Efremova, M., Krabichler, B., Speicher, M.R., Zschocke, J., and Trajanoski, Z. (2014). A survey of tools for variant analysis of next-generation genome sequencing data. Briefings in Bioinformatics *15*, 256–278.

17. Girard, S.L., Gauthier, J., Noreau, A., Xiong, L., Zhou, S., Jouan, L., Dionne-Laporte, A., Spiegelman, D., Henrion, E., Diallo, O., et al. (2011). Increased exonic de novo mutation rate in individuals with schizophrenia. Nature Publishing Group 1–5.

18. Veeramah, K.R., Johnstone, L., Karafet, T.M., Wolf, D., Sprissler, R., Salogiannis, J., Barth-Maron, A., Greenberg, M.E., Stuhlmann, T., Weinert, S., et al. (2013). Exome sequencing reveals new causal mutations in children with epileptic encephalopathies. Epilepsia *54*, 1270–1281.

19. Vissers, L.E.L.M., de Ligt, J., Gilissen, C., Janssen, I., Steehouwer, M., de Vries, P., van Lier, B., Arts, P., Wieskamp, N., del Rosario, M., et al. (2010). A de novo paradigm for mental retardation. Nature Publishing Group *42*, 1109–1112.

20. Michaelson, J.J., Shi, Y., Gujral, M., Zheng, H., Malhotra, D., Jin, X., Jian, M., Liu, G., Greer, D., Bhandari, A., et al. (2012). Whole-Genome Sequencing in Autism Identifies Hot Spots for De Novo Germline Mutation. Cell *151*, 1431–1442.

21. Lek, M., Karczewski, K., Minikel, E., Samocha, K., and Banks, E. (2016). Analysis of protein-coding genetic variation in 60,706 humans. bioRxiv.

22. Chen, L., Liu, P., Evans, T.C.J., and Ettwiller, L. (2016). DNA Damage is the driving force of sequencing error. Biology of Genomes.

23. Howell, N., Smejkal, C.B., Mackey, D.A., Chinnery, P.F., Turnbull, D.M., and

bioRxiv preprint first posted online Jul. 26, 2016; doi: http://dx.doi.org/10.1101/066043. The copyright holder for this preprint (which was not peer-reviewed) is the author/funder. All rights reserved. No reuse allowed without permission.

Herrnstadt, C. (2003). The pedigree rate of sequence divergence in the human mitochondrial genome: there is a difference between phylogenetic and pedigree rates. The American Journal of Human Genetics *72*, 659–670.

24. Wall, J.D., Cox, M.P., Mendez, F.L., Woerner, A., Severson, T., and Hammer, M.F. (2008). A novel DNA sequence database for analyzing human demographic history. Genome Research *18*, 1354–1361.

25. Kloss-Brandstätter, A., Pacher, D., Schönherr, S., Weissensteiner, H., Binna, R., Specht, G., and Kronenberg, F. (2011). HaploGrep: a fast and reliable algorithm for automatic classification of mitochondrial DNA haplogroups. Hum. Mutat. *32*, 25–32.

26. Drmanac, R., Sparks, A.B., Callow, M.J., Halpern, A.L., Burns, N.L., Kermani, B.G., Carnevali, P., Nazarenko, I., Nilsen, G.B., Yeung, G., et al. (2010). Human genome sequencing using unchained base reads on self-assembling DNA nanoarrays. Science *327*, 78–81.

27. Auton, A., Abecasis, G.R., Altshuler, D.M., Durbin, R.M., Abecasis, G.R., Bentley, D.R., Chakravarti, A., Clark, A.G., Donnelly, P., Eichler, E.E., et al. (2015). A global reference for human genetic variation. Nature *526*, 68–74.

28. Andrews, R.M., Kubacka, I., Chinnery, P.F., Lightowlers, R.N., Turnbull, D.M., and Howell, N. (1999). Reanalysis and revision of the Cambridge reference sequence for human mitochondrial DNA. Nature Genetics *23*, 147.

29. Anderson, S., Bankier, A.T., Barrell, B.G., de Bruijn, M.H., Coulson, A.R., Drouin, J., Eperon, I.C., Nierlich, D.P., Roe, B.A., Sanger, F., et al. (1981). Sequence and organization of the human mitochondrial genome. Nature *290*, 457–465.

30. Li, H., and Durbin, R. (2009). Fast and accurate short read alignment with Burrows-Wheeler transform. Bioinformatics *25*, 1754–1760.

31. McKenna, A., Hanna, M., Banks, E., Sivachenko, A., Cibulskis, K., Kernytsky, A., Garimella, K., Altshuler, D., Gabriel, S., Daly, M., et al. (2010). The Genome Analysis Toolkit: A MapReduce framework for analyzing next-generation DNA sequencing data. Genome Research *20*, 1297–1303.

32. van Oven, M., and Kayser, M. (2009). Updated comprehensive phylogenetic tree of global human mitochondrial DNA variation. Hum. Mutat. *30*, E386–E394.

33. O'Rawe, J., Guangqing, S., Wang, W., Hu, J., Bodily, P., Tian, L., Hakonarson, H., Johnson, E., Wei, Z., Jiang, T., et al. (2013). Low concordance of multiple variant-calling pipelines: practical implications for exome and genome sequencing. Genome Med *5*, 28.

34. Degner, J.F., Marioni, J.C., Pai, A.A., Pickrell, J.K., Nkadori, E., Gilad, Y., and Pritchard, J.K. (2009). Effect of read-mapping biases on detecting allele-specific expression from RNA-sequencing data. Bioinformatics *25*, 3207–3212.

bioRxiv preprint first posted online Jul. 26, 2016; doi: http://dx.doi.org/10.1101/066043. The copyright holder for this preprint (which was not peer-reviewed) is the author/funder. All rights reserved. No reuse allowed without permission.

35. Rasmussen, M.D., Hubisz, M.J., Gronau, I., and Siepel, A. (2014). Genome-Wide Inference of Ancestral Recombination Graphs. PLoS Genet *10*, e1004342.

36. Veeramah, K.R., Wegmann, D., Woerner, A., Mendez, F.L., Watkins, J.C., Destro-Bisol, G., Soodyall, H., Louie, L., and Hammer, M.F. (2012). An Early Divergence of KhoeSan Ancestors from Those of Other Modern Humans Is Supported by an ABC-Based Analysis of Autosomal Resequencing Data. Mol Bio Evol *29*, 617–630.

37. Henn, B.M., Botigué, L.R., Peischl, S., Dupanloup, I., Lipatov, M., Maples, B.K., Martin, A.R., Musharoff, S., Cann, H., Snyder, M.P., et al. (2016). Distance from sub-Saharan Africa predicts mutational load in diverse human genomes. Proceedings of the National Academy of Sciences *113*, E440–E449.

38. Durbin, R.M., Altshuler, D.L., Durbin, R.M., Abecasis, G.R., Bentley, D.R., Chakravarti, A., Clark, A.G., Collins, F.S., La Vega, De, F.M., Donnelly, P., et al. (2010). A map of human genome variation from population-scale sequencing. Nature *467*, 1061–1073.

39. Rebolledo-Jaramillo, B., Su, M.S.-W., Stoler, N., McElhoe, J.A., Dickins, B., Blankenberg, D., Korneliussen, T.S., Chiaromonte, F., Nielsen, R., Holland, M.M., et al. (2014). Maternal age effect and severe germ-line bottleneck in the inheritance of human mitochondrial DNA. Proceedings of the National Academy of Sciences *111*, 15474–15479.

bioRxiv preprint first posted online Jul. 26, 2016; doi: http://dx.doi.org/10.1101/066043. The copyright holder for this preprint (which was not peer-reviewed) is the author/funder. All rights reserved. No reuse allowed without permission.

Figure Legends:

Figure 1: **Two Schematics Illustrating False Negative Identification**. A) A schematic representation of (1) the process that was used to obtain mitochondrial SNV data for each individual (before the "assign to tree" arrow) and (2) the algorithm that was used to identify false negatives in such data (*i.e*. SNVs that should have been present, but were not) based on an independently obtained phylogenetic tree (phylotree.org). B) Schematic summarizing NGS false negative identification with Sanger validation. Each box summarizes the steps and data formats that were used to identify NGS false negatives assuming that the Sanger sequenced fragments represented the true variation.

Figure 2: Histogram of mtDNA False Negatives by Chromosomal Location. Grey bars indicate areas of repetitive sequence on the mitochondrial chromosome, obtained by the application of RepeatMasker (including simple repeats) to the mitochondrial sequence.

Figure 3: Autosomal False Negative Sites by Coverage and Allele Frequency. Each dot represents an NGS autosomal false negative (FN) site in one individual from the single-sample variant calling dataset. FNs are colored by project (Table 1). The Complete Genomics dataset has higher mean coverage than the two Illumina datasets in our study. To calculate allele frequency, Sanger data from the three African populations were combined and the allele frequency across the dataset was estimated as the non-reference allele frequency. The y-axis represents the non-reference allele frequency relative to hg19. False negatives span the full frequency range in all three datasets.

Table 1: *Autosomal False Negative Rates Assessed from Sanger Sequencing*

Table 2: *Candidate de novo mitochondrial mutations from 131 duos*

bioRxiv preprint first posted online Jul. 26, 2016; doi: http://dx.doi.org/10.1101/066043. The copyright holder for this preprint (which was not peer-reviewed) is the author/funder. All rights reserved. No reuse allowed without permission.

Figures & Tables

Figure 1:

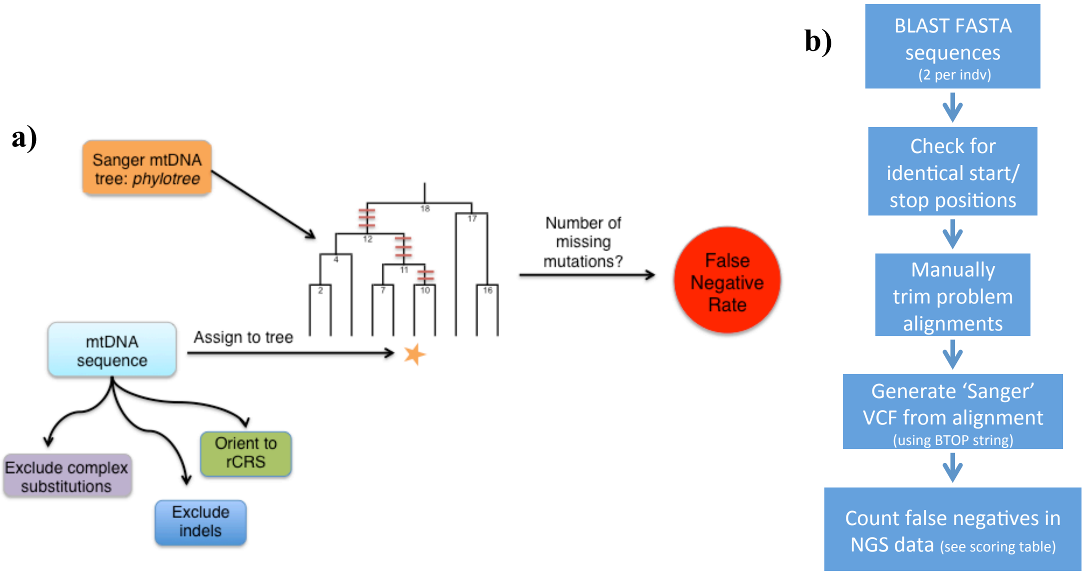
a)
Sanger mtDNA tree: *phylotree*
18
17
12
4
11
2
7
10
16
Number of missing mutations?
False Negative Rate
mtDNA sequence
Assign to tree
Exclude complex substitutions
Orient to rCRS
Exclude indels
b)
BLAST FASTA sequences (2 per indv)
Check for identical start/ stop positions
Manually trim problem alignments
Generate 'Sanger' VCF from alignment (using BTOP string)
Count false negatives in NGS data (see scoring table)

bioRxiv preprint first posted online Jul. 26, 2016; doi: http://dx.doi.org/10.1101/066043. The copyright holder for this preprint (which was not peer-reviewed) is the author/funder. All rights reserved. No reuse allowed without permission.

Figure 2:

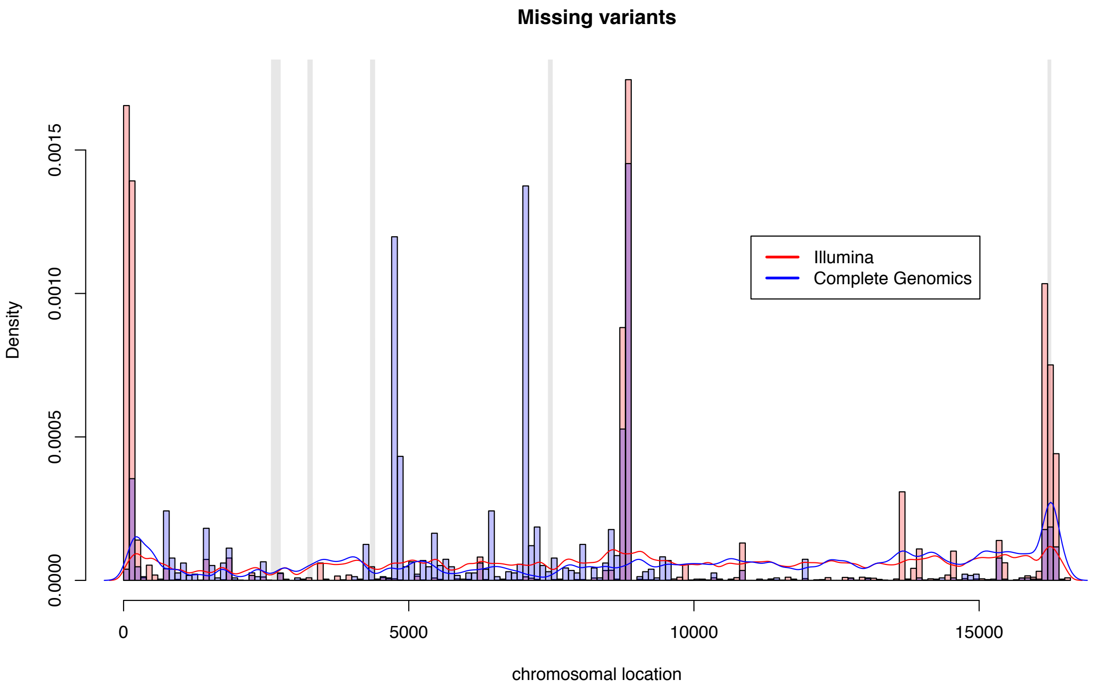

bioRxiv preprint first posted online Jul. 26, 2016; doi: http://dx.doi.org/10.1101/066043. The copyright holder for this preprint (which was not peer-reviewed) is the author/funder. All rights reserved. No reuse allowed without permission.

Figure 3:

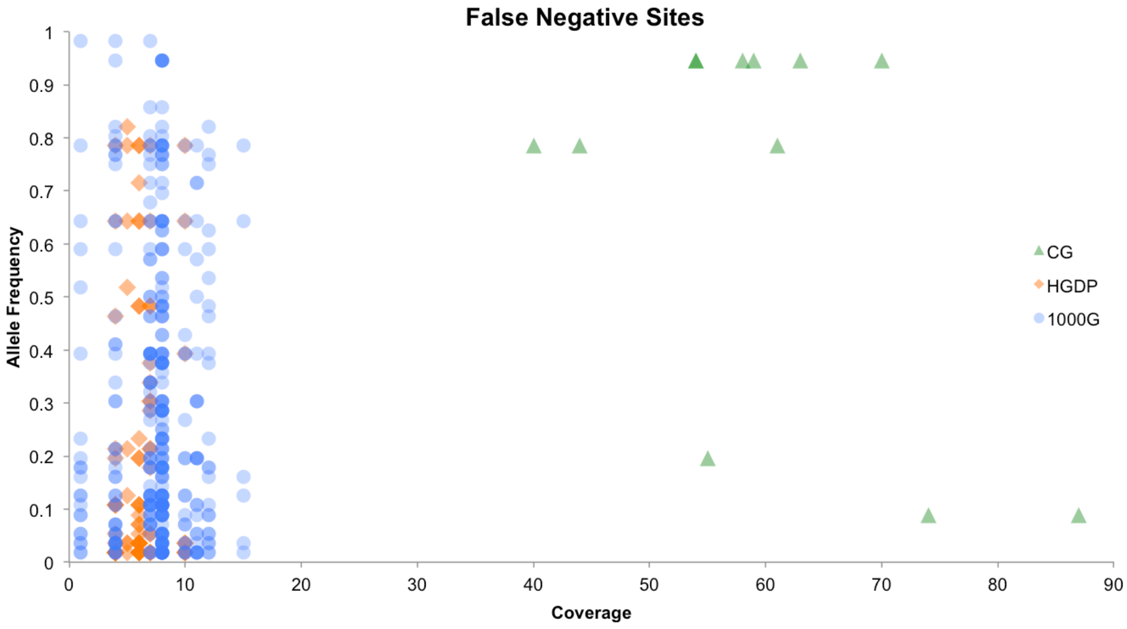

bioRxiv preprint first posted online Jul. 26, 2016; doi: http://dx.doi.org/10.1101/066043. The copyright holder for this preprint (which was not peer-reviewed) is the author/funder. All rights reserved. No reuse allowed without permission.

Table 1: *Autosomal False Negative Rates Assessed from Sanger Sequencing*

Population	**Sample ID**	**Multi-sample Imputed**		**Multi-sample Unimputed**		**Single-sample Calls**	
		FN[1]	**FP[2]**	**FN[1]**	**FP[2]**	**FN[1]**	**FP[2]**
LWK (1000G)	NA19027	-	-	-	-	12.1%	3.30%
	NA19028	6.0%	0.0%	-	-	18.8%	2.01%
	NA19041	8.1%	0.7%	-	-	14.9%	2.70%
	NA19044	6.3%	1.2%	-	-	29.9%	2.87%
	NA19046	5.0%	0.6%	-	-	32.0%	2.87%
	NA19307	9.3%	0.6%	-	-	15.4%	1.65%
	NA19308	7.0%	0.0%	-	-	4.7%	0.58%
	NA19309	6.0%	0.0%	-	-	11.1%	1.51%
	NA19317	4.2%	0.6%	-	-	18.1%	3.01%
	NA19319	5.1%	0.6%	-	-	14.2%	1.70%
	NA19346	3.1%	0.0%	-	-	19.8%	0.62%
	NA19350	5.3%	0.0%	-	-	22.3%	0.97%
	NA19360	3.9%	0.6%	-	-	12.8%	1.67%
	NA19371	9.6%	2.3%	-	-	31.5%	3.93%
	NA19373	6.3%	0.0%	-	-	21.4%	3.14%
	NA19380	3.9%	1.7%	-	-	13.7%	3.30%
	Mean (SD)	**5.9%** ±0.5%	**0.6%** ±0.2%	**-**	**-**	**18.3%** ±1.9%	**2.2%** ±0.3%
MBI (HGDP)	HGDP00449	7.4%	1.0%	5.0%	2.0%	8.4%	3.5%
	HGDP00456	4.7%	0.05%	2.6%	1.6%	3.2%	2.1%
	HGDP00462	13.6%	1.6%	4.2%	1.6%	12.6%	2.1%
	HGDP00471	6.9%	0.6%	1.3%	0.6%	6.3%	1.3%
	HGDP00474	6.6%	1.5%	4.1%	0.5%	4.6%	2.6%
	HGDP00476	13.2%	1.5%	2.9%	1.0%	10.8%	5.9%
	Mean (SD)	**8.8%** ±1.5%	**1.1%** ±0.6%	**3.3%** ±0.6%	**1.2%** ±1.7%	**7.6%** ±1.5%	**2.9%** ±0.7%
YRI (1000G)[3] (CG)[3]	NA18501	2.9%	0.0%	-	-	9.4%	0.0%
	NA18502	1.7%	0.0%	-	-	9.6%	0.0%
	NA18505	4.6%	0.0%	-	-	9.9%	0.0%
	NA18517	1.6%	0.0%	-	-	0.0%	0.0%
	NA19238	-	-	-	-	9.4%	0.0%
	NA19239	-	-	-	-	8.7%	0.0%
	Mean (SD)	**2.7%** ±1.4%	**0.0%**	**-**	**-**	**7.8%** ±1.6%	**0.0%**

[1] Indicates the false negative rate as assessed from comparison to 80 kilobases of Sanger sequencing from the same individual.

[2] Indicates the false positive rate as assessed from comparison to 80 kilobases of Sanger sequencing from the same individual. We assume the Sanger sequencing does not contain spurious mutational errors.

[3] The multi-sample imputed column represents low-coverage data from 1000G; the single-sample column represents the high-coverage Complete Genomes data.

bioRxiv preprint first posted online Jul. 26, 2016; doi: http://dx.doi.org/10.1101/066043. The copyright holder for this preprint (which was not peer-reviewed) is the author/funder. All rights reserved. No reuse allowed without permission.

Table 2: *Candidate de novo mitochondrial mutations from 131 duos*

Mother ID	Child ID	Source	Haplogroup Assignment	Candidate *de novo* mutation[1]	FP in child due to 'No call' in Mother[2]	FP in child due to FN in Mother[3]
GS000016020	GS000016048	LCL	U4b1b1	8655 (242)		
				10566 (22)		
GS000016039	GS000016539	LCL	H2a5b / H2a5	**9835** (8342)	3166 (7413)	
GS000016041	GS000016538	LCL	U5b2a1a+16311 / U5b2	**204** (9262)		
GS000016398	GS000016412	LCL	T2 / T2b	14050 (629)		
GS000016456	GS000016408	LCL	H52	2351 (2147)		
GS000016465	GS000016380	LCL	H5b1	**279** (13042)		
				14569 (8028)		
GS000017172	GS000017223	LCL	L3e2b1a2	2045 (1342)	2483 (73)	16189 (516, L3e2b)
GS000017130	GS000017271	Blood	B2	3173 (2494)		
GS000016414	GS000016400	LCL	U5a1a2b		750 (2424)	1700 (6051, U5a1a)
					1438 (1584)	3197 (17404, U5a'b)
					2706 (10860)	11467 (6271, U)
					10915 (8882)	14793 (8883, U5a)
					14766 (4244)	15218 (8736, U5a1)
					15326 (10230)	
GS000016469	GS000016540	LCL	H3a1a		4769 (129)	
GS000017276	GS000017275	Buffy	L1b1a15		3936 (1003)	
GS000016396	GS000016409	LCL	U3a1a/U3a1		8860 (205)	
GS000016011	GS000016459	LCL	W1c1		2706 (12255)	
					4769 (305)	
GS000017242	GS000016026	LCL	U5a1		2706 (11788)	
					8994 (1864)	
GS000017185	GS000017173	LCL	L2a1f			16192 (4551, L2a1f)
GS000017227	GS000017119	LCL	L2b3a			16213 (6945, L2b)
GS000017045	GS000017047	Buffy	L1b1a15			16355 (6228, L1b1a15)
			Total count	**10**	**15**	**9**

[1] Mitochondrial base pair position for each candidate *de novo* mutation which appeared in the child but not the mother. The variant quality score for the child's SNV is indicated in parentheses. Quality scores greater than 5000 are indicated in bold (see supplemental Figure S3 for bimodal distribution of variant quality scores).

[2] mtDNA position of candidate *de novo* mutations which were inferred to be false positives due to a 'no call' in the mother. The variant quality score for the child's SNV is indicated in parentheses.

[3] mtDNA position of candidate *de novo* mutations which were inferred to be false positives in the child inferred from the local mtDNA phylogeny; mother's allele was indicated as reference but the mutation was derived in the derived haplogroup (i.e. a haplogroup defining mutation). Haplogroup defined in parentheses.

bioRxiv preprint first posted online Jul. 26, 2016; doi: http://dx.doi.org/10.1101/066043. The copyright holder for this preprint (which was not peer-reviewed) is the author/funder. All rights reserved. No reuse allowed without permission.